

# Multiphysics simulations of thermoelectric generator modules with cold and hot blocks and effects of some factors



W. Li<sup>a,\*</sup>, M.C. Paul<sup>a,\*</sup>, A. Montecucco<sup>a</sup>, J. Siviter<sup>a</sup>, A.R. Knox<sup>a</sup>, T. Sweet<sup>b</sup>, M. Gao<sup>b</sup>,  
H. Baig<sup>c</sup>, T.K. Mallick<sup>c</sup>, G. Han<sup>d</sup>, D.H. Gregory<sup>d</sup>, F. Azough<sup>e</sup>, R. Freer<sup>e</sup>

<sup>a</sup> School of Engineering, University of Glasgow, Glasgow G12 8QQ, UK

<sup>b</sup> School of Engineering, Cardiff University, Cardiff CF24 3AA, UK

<sup>c</sup> The Environment and Sustainability Institute, University of Exeter, Penryn TR10 9FE, UK

<sup>d</sup> WestCHEM, School of Chemistry, University of Glasgow, Glasgow G12 8QQ, UK

<sup>e</sup> School of Materials, University of Manchester, Manchester M13 9PL, UK

## ARTICLE INFO

### Keywords:

Thermoelectric generator  
Thermal and electrical analysis  
Radiation  
Heat transfer  
Multiphysics simulation

## ABSTRACT

Transient and steady-state multiphysics numerical simulations are performed to investigate the thermal and electrical performances of a thermoelectric generator (TEG) module placed between hot and cold blocks. Effects of heat radiation, leg length and Seebeck coefficient on the TEG thermal and electrical performances are identified. A new correlation for the Seebeck coefficient with temperature is proposed. Radiation effects on the thermal and electric performances are found to be negligible under both transient and steady-state conditions. The leg length of the TEG module shows a considerable influence on the electrical performance but little on the thermal performance under transient conditions. A nearly linear temperature profile on a leg of the TEG module is identified. The temperature profile of the substrate surfaces is non-uniform, especially in the contacted areas between the straps (tabs) and the substrates.

## 1. Introduction

An integrated or hybrid compound parabolic concentrator (CPC) with photovoltaic (PV) and other thermal techniques have been proposed recently to improve the solar energy utilisation efficiency potentially. Conventional concentrated solar power technologies were reviewed and applicability particularly in West African countries was discussed in [1]. The effects of a CPC trough and thermal collector on the electrical performance of a solar panel were analysed in [2], and a solar cell with a CPC trough was cooled by two air streams through the CPC and fins installed on the back cover of the cell as demonstrated in [3,4].

A hybrid photovoltaic-thermal water heating system was developed recently for residential applications [5,6]. The system was subject to 37.6–48.65% thermal and 10.3–12.3% electrical efficiencies. In [7], a silicon thin-film solar cell, thermoelectric generator (TEG) and heat collector were integrated together. A solar TEG was also proposed by Amatya and Ram [8] for micro-power applications by means of a cheap parabolic concentrator. CPC, solar module and thermal collectors were incorporated together in [9], resulting in a 62–67.9% averaged optical efficiency per day. An analytical model for solar module with CPC and TEG devices was established in [10] and the effects of thermal conductance between the module and the TEG, current of module, irradiance, concentration ratio and figure of merit of TEG on performance were studied. In [11], a TEG, CPC and heat exchanger were integrated together to form a hybrid electric/thermal energy conversion device with the best conversion efficiencies, 0.6% and 43.3% in

\* Corresponding author.

E-mail addresses: [Wenguang.Li@glasgow.ac.uk](mailto:Wenguang.Li@glasgow.ac.uk) (W. Li), [Manosh.Paul@glasgow.ac.uk](mailto:Manosh.Paul@glasgow.ac.uk) (M.C. Paul).

<http://dx.doi.org/10.1016/j.csite.2017.03.005>

Received 5 October 2016; Accepted 22 March 2017

Available online 23 March 2017

2214-157X/ © 2017 The Authors. Published by Elsevier Ltd. This is an open access article under the CC BY license (<http://creativecommons.org/licenses/by/4.0/>).

electricity and thermal energy at a water flow rate of 0.24 kg/s, respectively.

In our funded project, we aim to develop an integrated CPC, PV, TEG and other thermal techniques for a further increase working efficiency of a PV module. In doing so, a numerical method is needed to characterize the steady-state and transient thermal and electrical performance of a TEG module when the temperature, geometrical and electrical parameters of the TEG are varied.

Previously, the modelling of the TEG module was carried out by using 1D simulation methods usually applied to a single thermocouple (two legs) [12–16]. These models were developed for simulator software such as SPICE [12,13], Modelica [14], and MATLAB/Simulink [15,16] and they were capable of predicting electrical and thermal performance of the TEG. An unsteady heat conduction model with Joule heat generation for a TEG was also developed in [17] to study the transient thermal performance, while Alata et al. [18] developed a hyperbolic heat conduction model and investigated the dynamic thermal behaviour of a TEG. Nguyen and Pochiraju [19] considered both the Joule heating and Thomson effects. The TEG model with constant thermal and electrical properties was subject to variable heat sources.

More recently, thermal and electrical finite element methods were applied into TEG modules without a heater and heat sink in [20–26]. The method in [20] was applied to a single pellet and a parametric analysis of a multi-stage Peltier cooler was presented. The steady cooling performance of a thermo-electrical micro-cooler was analysed in [21] using COMSOL. The geometrical parameters of the cooler were optimised under various temperature differences without thermal and electrical contact effects. The leg and thermal and electrical properties of the TEG were inversely determined with an approach based on experiments and finite element least squares in [22]. Chen et al. [23] used the 3D finite volume method in ANSYS 12.0.1 and investigated steady-state performance of a miniature thermo-electrical cooler with and without considering the Thomson effect. The thermal and electrical properties of the legs were variable with temperature, however, the thermal and electrical contacts were neglected. ANSYS was also applied by Xiao et al. [24] to characterise the steady electrical performance of one- and two-stage TEGs with different materials, but the thermal and electrical properties were constant again and without thermal and electrical contact effects. Thermal stress and deformation in TEG module legs were estimated by using finite element analysis in [25,26] and high stress concentration and large deformation were found on the edges of the TEG contact with the hot substrate.

The studies above are obviously fruitful and respected. However, in these steady thermal and electrical performance simulations, the heater (hot block) and heat exchanger (cold block) of a TEG module have not been considered. Even though a transient thermal and electrical performance of a TEG module with heater and heat exchanger was conducted in [27], the effects of leg length and the Seebeck coefficient, steady performance, and mesh independence study were not involved. The temperature along the leg of the TEG was also not demonstrated.

In this article, we study the transient thermal and electrical performance of a TEG system comprising a TEG, heater (hot block) and heat exchanger (cold block) by means of ANSYS 15.0 Thermal-Electric System. Additionally, the thermal and electrical contacts as well as radiation effects are taken into account. To characterise the TEG module performance, results are presented for a number of important variables such as temperature, Joule heat, electrical current and voltage profile in the TEG. The temperature along one leg of the TEG is shown to demonstrate the thermal and electrical coupling effect. A new scaled Seebeck coefficient for  $\text{Bi}_2\text{Te}_3$  is also proposed.

## 2. Models, boundary conditions and methods

### 2.1. Computational models

The experimental test rig and instrument shown in Fig. 1(a)–(c) were developed in [28] to characterise various TEG modules suitable for solar energy harvesting systems. The experimental set-up consists of a cold block with cooling water pipes, TEG module, hot block with an electric heater, a vermiculite insulating layer, a bottom steel plate, and a top load cell/sensor which is used to measure a force applied on the cold block. By using this force the hot block, TEG and cold block can be held together firmly. Experimental data were collected from the load cell, thermal couplings installed in the heat exchanger inlets and outlets, on the TEG top substrate contacted with the cold block, on the TEG bottom substrate attached to the hot block and on a surface of the heater by a data logger connected to a PC. This set-up allows measurement of both transient and steady-state thermal and electric performance of the TEG module.

The method for measuring the electric performance of a TEG module has been described completely in [28]. The main idea is to pick up the current and voltage through and across a TEG module when the electrical current load in an external electrical circuit connected with the module is changed with a certain step from open-circuit operating point to short-circuit point at a specific temperature difference across the module. The control program used in the electrical experiment was able to check the temperature difference based on the signals from the thermocouples and control the current in the heater. The prescribed mechanical loading generated by a spring applied on the load cell/sensor remains constant during the electrical experiment.

We characterised the thermal and electrical performance of the TEG model GM250-127-14-10 (European Thermodynamics Ltd) by means of ANSYS 15.0 Thermal-Electric System and compared results with those presented in [29]. The computational model includes a load sensor, a cold block, a TEG module, and a hot block, as shown in Fig. 1(d). The hot and cold blocks are subject to conductive heat transfer, while the TEG module experiences a coupled thermoelectricity process.

The governing equations of conductive heat transfer and thermoelectricity are detailed in [20], including the Peltier and Thomson effects. The steady continuity of electrical current density and the coupled heat transfer and thermoelectricity equations in the isotropic and homogenous legs, copper straps and leads are as follows [20]:

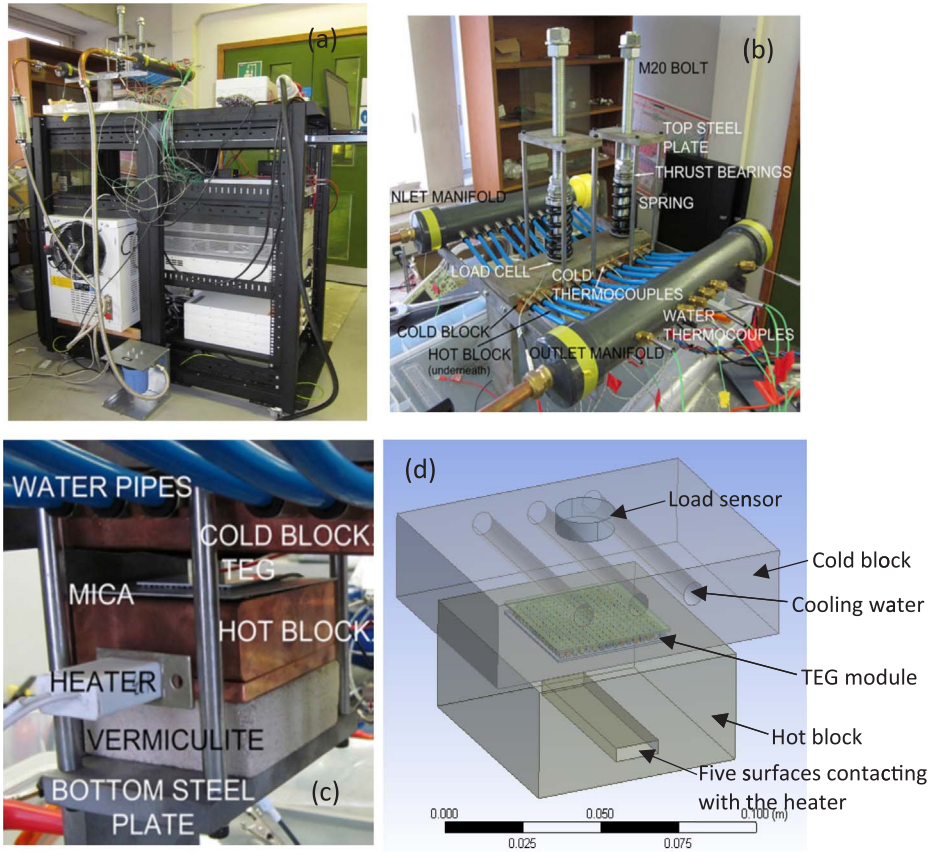


Fig. 1. Experimental set-up outlook in [28] (a), a force applying device on the cold block to hold the cold block, TEG module and hot block together, the load cell/sensor measures a force magnitude applied (b), a close-up view of the cold block, TEG module and hot block (c) and the computational model (d).

$$\nabla \cdot \mathbf{J} = 0 \tag{1}$$

$$\rho C \frac{\partial T}{\partial t} + \nabla \cdot (\alpha T \mathbf{J}) - \nabla \cdot (k \nabla T) = s \tag{2}$$

$$\nabla \cdot \left( \frac{\alpha}{r} \nabla T \right) + \nabla \cdot \left( \frac{1}{r} \nabla \varphi \right) = 0 \tag{3}$$

where  $\rho$ ,  $C$  and  $T$  are the density, specific heat capacity and temperature of the legs, straps, leads, substrates, hot and cold blocks, respectively. Note that the legs are the thermoelectric legs of a TEG module, the straps are the metal interconnects, which connect the different legs, and the leads are two leads connecting an external electrical circuit, while the substrates are surrounding ceramic plates.  $s$  is the heat generation rate per unit volume;  $\alpha$  is the Seebeck coefficient of two legs;  $k$  is the thermal conductivity of the legs, straps, leads, substrates, hot and cold blocks;  $r$  is the electric resistivity of the legs, straps and leads;  $\varphi$  is the electrical scalar potential in the legs, straps and leads; and  $\mathbf{J}$  is the electrical current density vector in the legs, straps and leads, which is related to the electrical scalar potential  $\varphi$  by

$$\mathbf{J} = \frac{1}{r} (-\nabla \varphi - \alpha \nabla T) \tag{4}$$

Note that the heat flux vector  $\mathbf{q}$  depends upon both the current density and temperature gradient in the legs, straps and leads, i.e.

$$\mathbf{q} = \alpha T \mathbf{J} - k \nabla T \tag{5}$$

Since the hot and cold blocks as well as substrates are dielectric,  $\mathbf{J} = 0$ ,  $r = \infty$  and  $\varphi = \text{constant}$  were set; as a result only Eq.(1) is solved for heat transfer. However, in the legs, straps and leads, Eqs. (1) and (2) are solved in a coupled manner. In ANSYS 15.0 Thermal-Electric System both thermal and electrical processes are considered to be steady-state. Therefore, the transient performance of the TEG obtained here is based on the evolution of a series of steady-state solutions, i.e. quasi-steady solutions, under various heater temperatures and electrical current densities in the lead.

The thermal and electrical properties of the materials of the hot and cold block, TEG module and sensor are isotropic and homogenous, and listed in Table 1. Note that the thermal conductivity, resistivity and Seebeck coefficient are temperature-dependent, thus the corresponding equations used are also shown underneath Table 1.

**Table 1**  
Thermal and electrical properties of materials.

Component	Material	Density $\rho$ (kg/m <sup>3</sup> )	Specific heat capacity $C$ (J/(kg K))	Thermal conductivity $k$ (W/(m K))	Emissivity $\epsilon$	Resistivity $r$ (ohm m)	Seebeck coefficient $\alpha$ (V/K)
Load cell	steel	7750	480	15	0.35	N/A	N/A
Cold block	copper	8300	385	401	0.07	N/A	N/A
Hot block							
TEG Strap lead	copper	8300	385	401	N/A	$1.69 \times 10^{-8}$	N/A
substrate	ceramic	3220	419	31	0.6	N/A	N/A
n, p-legs	Bi <sub>2</sub> Te <sub>3</sub>	7740	200	a	0.9	b	c

a  $k = (62605 - 277.7T + 0.4131T^2) \times 10^{-6}$

b  $r = (5112 + 163.4T + 0.6279T^2) \times 10^{-8}$

c  $\alpha = (22224 + 930.6T - 0.9905T^2) \times 10^{-9}$  after [30] and temperature  $T$  in K.

**2.2. Boundary conditions**

In the experimental set-up, the TEG is thermally driven by an electric heater which is installed inside the hot block. The heater, a thin cylinder with rectangular cross-section, is made of ceramics with an electrical resistor inside. The five surfaces of the heater contact with another five surfaces firmly inside the hot block and conduct the heat generated by the resistor to the hot block. Thermodynamics or electrodynamics of the heater is not modelled and removed from the geometrical model here, but the temperature on the five surfaces contacting with the heater in the hot block established by the heater under a certain condition is provided in the model instead, see Fig. 1(d).

In the transient simulation, the transient temperature profile against time illustrated in Fig. 2(a) according to the experimental data from [29] is applied on the surfaces contacting with the heater in the hot block. In the steady-state analysis, however, it is assumed that the heater has a uniform temperature over its surfaces, thus a constant temperature is assigned to the surfaces of the block in such a way that the temperature difference across the hot and cold substrates of the TEG is equal to 50, 100 and 150 °C.

In the transient analysis, the positive lead connecting with the n-leg, see Fig. 3, is subject to an electric current profile against time based on the experimental data [29], as shown in Fig. 2(b). In the steady-state analysis the current in the positive lead to the n-leg is constant in the range of 0–2.4 A. In the negative lead connecting with the p-leg, a zero voltage is always applied in both the transient and steady analyses. Note that because the electric current is just out of the positive lead, a negative electric current value is imposed in the lead in simulations.

The three holes in the cold block are for supplying cooling water at 19 °C and subject to a forced convection heat transfer coefficient of 1376.4 W/(m<sup>2</sup> °C) based on a conjugate heat transfer analysis conducted in ANSYS CFX in [31].

All the surfaces exposed with a surface temperature,  $T_{surface}$ , to air radiate heat into it with an emissivity  $\epsilon$  as shown in Table 1 at an ambient temperature  $T_{amb} = 19$  °C. Adopting the grey radiation model, the radiative heat flux to the ambient is written as [32]:

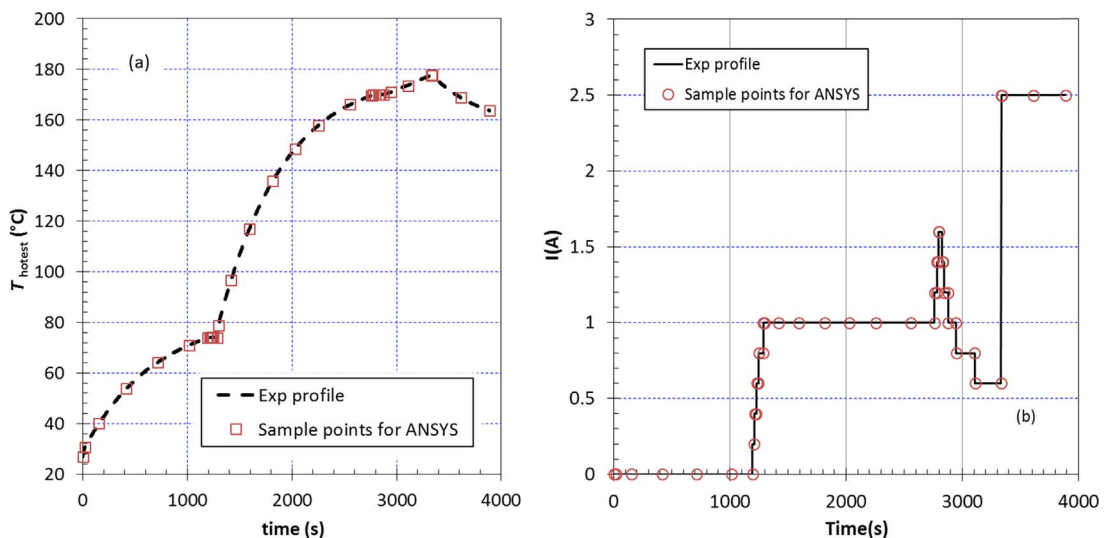


**Fig. 2.** Experimental highest temperature profile on the five heater surfaces(a), and electric current profile on the lead [29] (b). The symbols on the curves indicate the data used in the transient analysis.

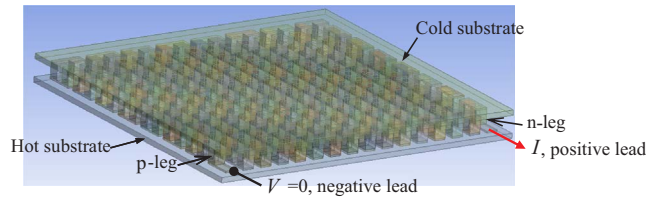


Fig. 3. Electric boundary conditions applied in the TEG module simulations.

$$q_{amb} = \epsilon\sigma(T_{surface}^4 - T_{amb}^4) \tag{6}$$

where  $\sigma$  is the Stefan-Boltzmann constant,  $\sigma = 5.670367 \times 10^{-8} \text{ kg s}^{-3}\text{K}^{-4}$ .

The bottom and side surfaces of the hot block are insulated with either stone or glass fibre. Thus they are subject to a negligible heat flux.

The other surfaces exposed to air, i.e. the load cell, the cold block and the TEG experience a natural convection with a coefficient of  $10 \text{ W}/(\text{m}^2 \text{ }^\circ\text{C})$  [31].

Thermal contacts are present in the interface between the sensor and the cold block, the cold block and the TEG substrate, the substrate and the strap, the substrate and the lead, the substrate and the hot block. Also, there is an electrical contact in the interface between the leg and strap, the leg and lead. The thermal and electrical contact conductance is given in Table 2.

### 2.3. Numerical methods

The computational domain is divided into 68,471 hexahedral (i.e. 3D 30-node hexahedrons in the legs, straps and substrates, sensor) and tetrahedral (i.e. 3D 10 node tetrahedrons in the hot and cold blocks) elements with 203,119 nodes, see Fig. 4. This is referred to as a fair mesh. A fine mesh is also generated, comprising of 306,404 elements and 1,459,557 nodes. The numbers of elements and nodes in the fine mesh are 4.47 and 7.19 times those in the fair mesh, respectively.

Simulations with two meshes are run at a temperature of  $205.28 \text{ }^\circ\text{C}$  on the five surfaces contacting with the heater in the hot block with a 3 A constant electrical current in the positive lead. The TEG thermal and electrical parameters are listed in Table 3. The thermal parameters no longer depend upon the mesh size, but the electrical parameters do with a relative maximum error of only 2.46% for the Joule heat. Thus the resolution used in the fair mesh is sufficient to get a high level of accuracy in the simulations while keeping the computational cost to a minimum, especially for the transient simulations which are usually time-intensive.

The heat conduction and thermoelectricity equations are discretised based on the finite element method with two degrees of freedom, i.e. temperature and electrical scalar potential or voltage on each node. The globally assembled matrix is asymmetrical and its nonlinear behaviour is solved with the Newton-Raphson method.

The converged criteria of heat flow and electric current are default settings such as  $3.653 \times 10^{-3}$  and  $5.795 \times 10^{-8}$ . The really achieved heat flow (W) and current (A) convergence values in simulations are  $1.261 \times 10^{-9}$  and  $4.036 \times 10^{-9}$ , respectively.

Table 2  
Thermal and electrical contact properties.

Contact interface	Component	Thermal conductance, $\text{W}/(\text{m}^2 \text{ }^\circ\text{C})$	Electric conductance, $\text{S}/\text{m}^2$	Reference
1	sensor cold block	3500	×	[33]
2	cold block substrate	3500	×	[33]
3	Hot block substrate	5500	×	[33]
4	substrate strap	50000	×	[33]
5	substrate lead	50000	×	[33]
6	strap leg	×	$10^9$	[34]
7	leg lead	×	$10^9$	[34]

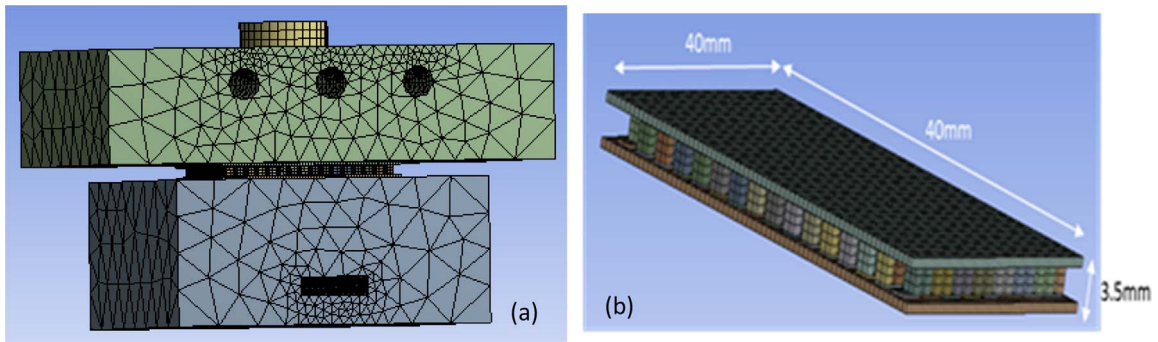


Fig. 4. Mesh pattern in the computational domains, (a) cold, hot blocks and TEG, (b) TEG.

### 3. Results

#### 3.1. Effects of leg length and radiation

The temperature difference and electrical power plots are shown in Fig. 5(a). The measured leg length and thickness of the TEG are 1.8 mm and 1.4 mm, respectively. The temperature on the hot side (hot substrate surface) of the TEG module is in good agreement with the experimental data. However, the temperature on the cold side (cold substrate surface) of the TEG is slightly over predicted after 1200 s when the load current increases from zero. With the exception of the time beyond 3300 s, simulation and experimental results for the temperature difference across the hot and cold sides of the TEG are in agreement. The predicted electrical power also matches the experimental curve, even though it is slightly over estimated.

The leg length constitutes an important factor affecting the electrical performance of the TEG. Presently, effects of leg length on the electric performance of a TEG model are mainly studied at a constant temperature difference and under the design condition where the external circuit electric resistance is equal to the electric resistance of a TEG itself [35] to achieve the maximum electric power for the TEG. The response of a TEG module with different leg lengths to the transient temperature difference and load current has not been investigated so far.

Therefore, two geometric models respectively with 2.0 mm and 1.6 mm leg length (varied by ± 11%) were generated and the same transient analysis was performed. The results are presented in Fig. 5 as well. It is seen that the leg length exhibits a significant effect on the electrical performance, but the thermal performance is little affected.

The radiation from hot surface to the air may affect the transient thermal and electrical performances. To identify this effect, the radiation is included in one transient simulation, and the temperature difference across the TEG and electrical are plotted in Fig. 5(b). It is seen that the radiation does not seem to have any remarked effect on both the performances and this finding is consistent with [36].

#### 3.2. Steady electrical performance and effect of the Seebeck coefficient

The steady-state electrical performance of the TEG module is presented at two constant temperature differences across its hot and cold sides with and without radiation effects. The voltage and electrical power curves, predicted at  $\Delta T = 50, 100$  and  $150\text{ }^\circ\text{C}$ , are displayed in Fig. 6(a) for the TEG module with a leg length of 1.8 mm. These results are compared with the experimental data from [29]. At  $\Delta T = 50$  and  $100\text{ }^\circ\text{C}$ , the predicted curves are consistent with the experimental data. But at  $\Delta T = 150\text{ }^\circ\text{C}$ , the voltage and electrical power are over predicted by about 10% due to a relatively large Seebeck coefficient used in this case. Once again, the radiation effect does not impact the performances. Hence the radiation can be ignored in the thermal and electrical simulations of a TEG module.

The over-estimation evinced in the results of Fig. 6(a), especially at a higher current, could be due to a Seebeck coefficient larger

Table 3  
TEG key parameters under different mesh sizes.

TEG Parameter	Fair mesh	Fine mesh	Relative error (%)
Temperature on hot substrate, $T_{hot}$ (°C)	189.72	189.70	-0.01
Temperature on cold substrate, $T_{cold}$ (°C)	39.72	39.71	+0.03
Temperature on hot strap, $T_{hot,strap}$ (°C)	183.32	183.24	-0.04
Temperature on cold strap, $T_{cold,strap}$ (°C)	52.90	52.93	-0.06
Voltage across leads, $V$ (V)	0.5081	0.5003	-1.54
Max Joule heat, (kW/m <sup>3</sup> )	$1.868 \times 10^4$	$1.822 \times 10^4$	-2.46

The temperature on the heater surfaces is  $205.28\text{ }^\circ\text{C}$ , the current in the leads is 3 A for two meshes; the scaled Seebeck coefficient presented by Eq.(8) is adopted in the computations.

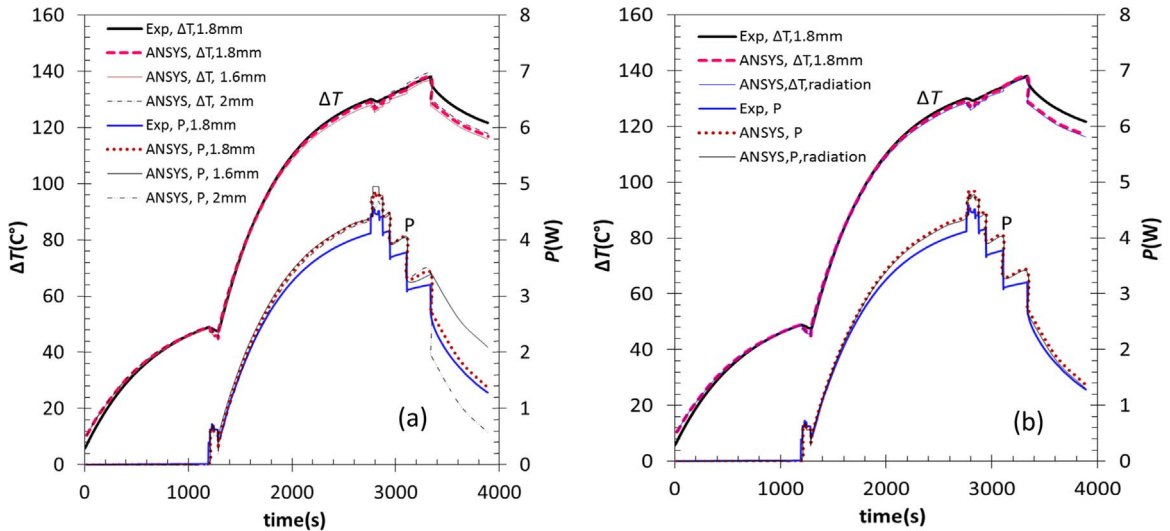


Fig. 5. Temperature difference and electric power curves for the TEG modules with 1.6 mm, 1.8 mm and 2 mm leg length without radiation (a) and the module with 1.8 mm leg length and radiation effect (b).

than the real one, since the predicted voltage axis intercept was higher than in the experimental data. Therefore the Seebeck coefficient,  $\alpha$ , proposed by Riffat et al. in [30] and presented in Table 1 with an expression, is scaled by a correction factor  $\chi$  which is expressed by a 2nd-order polynomial temperature:

$$\begin{cases} \alpha' = \chi \times \alpha \\ \chi = -6.5711 \times 10^{-6}T^2 + 4.0552 \times 10^{-3}T + 3.5084 \times 10^{-1} \end{cases} \quad (7)$$

where  $\chi$  is a correction factor to the Seebeck coefficient, and the temperature  $T$  is in K.

The steady performance curves with the corrected Seebeck coefficient are illustrated in Fig. 6(b). A better agreement between the predicted and experimental results is obtained and the voltage axis-intercepts are consistent with the experimental values. The predicted I-V curves at  $\Delta T = 50$  and  $100^\circ\text{C}$  are slightly steeper than the experimental ones, suggesting that the legs' internal electrical resistance ([30], Table 1) was slightly higher than the actual values at low temperature. A curve fitting method is then used to obtain a new correlation for the Seebeck coefficient that depends on temperature:

$$\alpha' = (-2.5844 \times 10^{-3}T^2 + 1.9122T - 1.3394 \times 10^2) \times 10^{-6} \quad (8)$$

where the corrected Seebeck coefficient  $\alpha'$  is in V/K. Note that this correlation is just applicable for our case. For other  $\text{Bi}_2\text{Te}_3$  materials it needs to be validated.

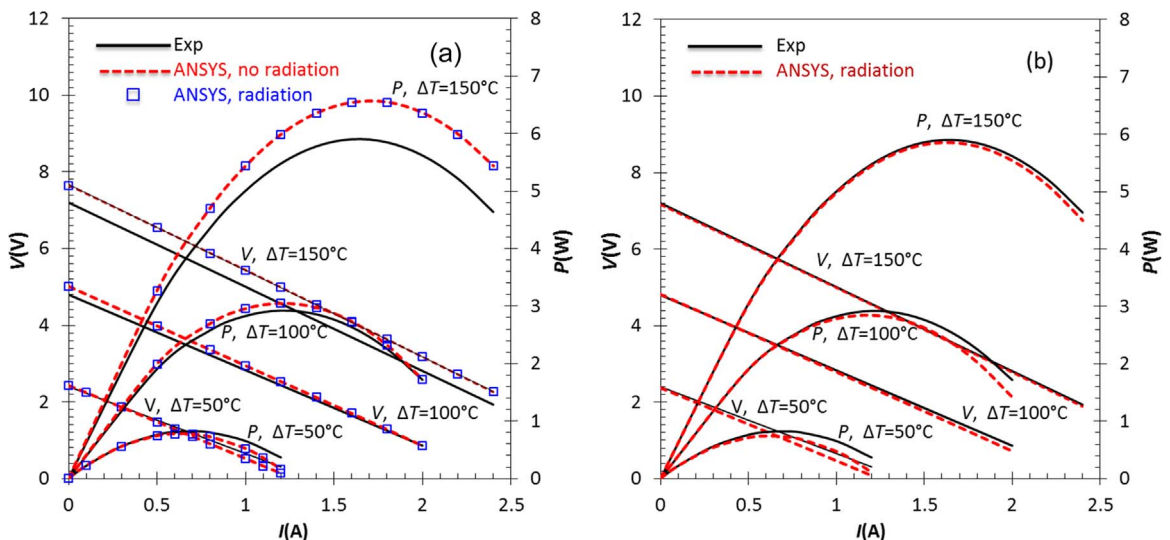


Fig. 6. Steady electric performance of the TEG module at 50, 100,  $150^\circ\text{C}$  temperature differences for the TEG with 1.8 mm leg length with and without radiation effects, (a) with Seebeck coefficient of Riffat et al. in [30], (b) with corrected Seebeck coefficient.

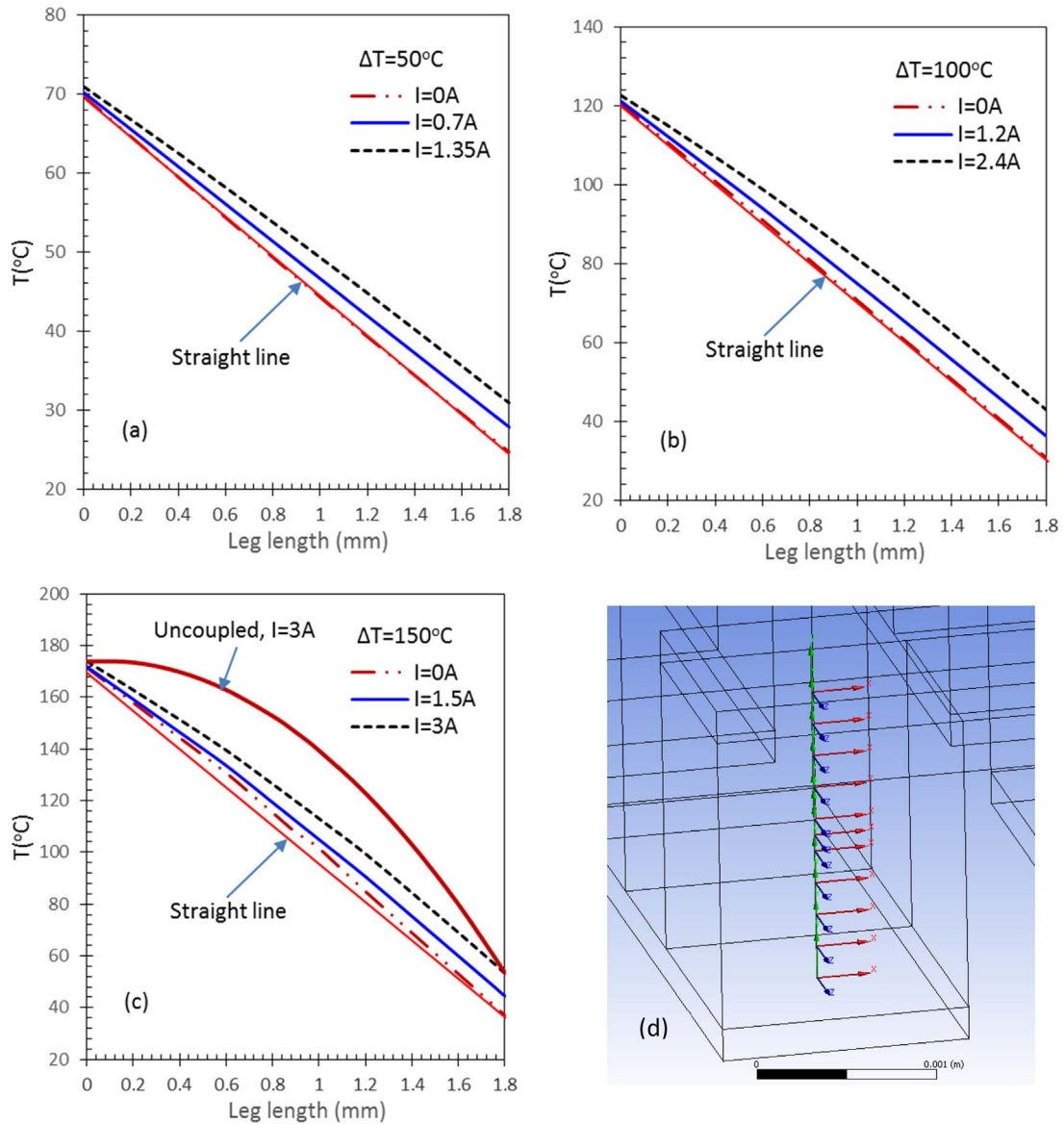


Fig. 7. Temperature profile shown on one leg along the central line of the TEG at three electric currents and  $\Delta T = 50, 100$  and  $150^{\circ}\text{C}$  with the scaled Seebeck coefficient (a–c). Measured points on the central line of the leg are shown in (d). The uncoupled solution is computed based on the equation provided in [17].

### 3.3. Temperature profile along leg

Since there is a thermal and electrical coupling in the TEG legs, the temperature profile with the coupling may be different from that under the thermal condition alone. To clarify this effect, eleven observation points are specified in one leg along the central line to cover the whole leg length, and the temperature on those points are recorded and plotted in Fig. 7 at three different electrical currents and  $\Delta T$  with the scaled Seebeck coefficient Eq. (8). It is found that the temperature profile exhibits a nonlinear behaviour at higher  $\Delta T$  and electrical current. However, when the temperature difference and the current drop, the profile approaches to a straight line asymptotically. This behaviour caused from the internal Joule heat generation in the TEG legs is consistent with the results presented in [17].

For further comparison, the temperature profile without the thermal and electrical coupling at  $\Delta T = 150^{\circ}\text{C}$  and  $I = 3\text{A}$  is illustrated in Fig. 7(c). This uncoupled solution is computed based on a 1D parabolic equation, i.e. the lumped model Eq.(3), presented in [17]. In the computation, the material properties and heat generation rate used are the mean values of them along the leg. The 1D uncoupled results showed a higher leg temperature, especially near the hot side. In the 3D simulations, the thermal and electrical coupling and free convection heat transfer around the TEG have been included. Thus the TEG is subject to a uniform temperature along the legs, leading to a small Seebeck coefficients and in turns a worse electrical performance.

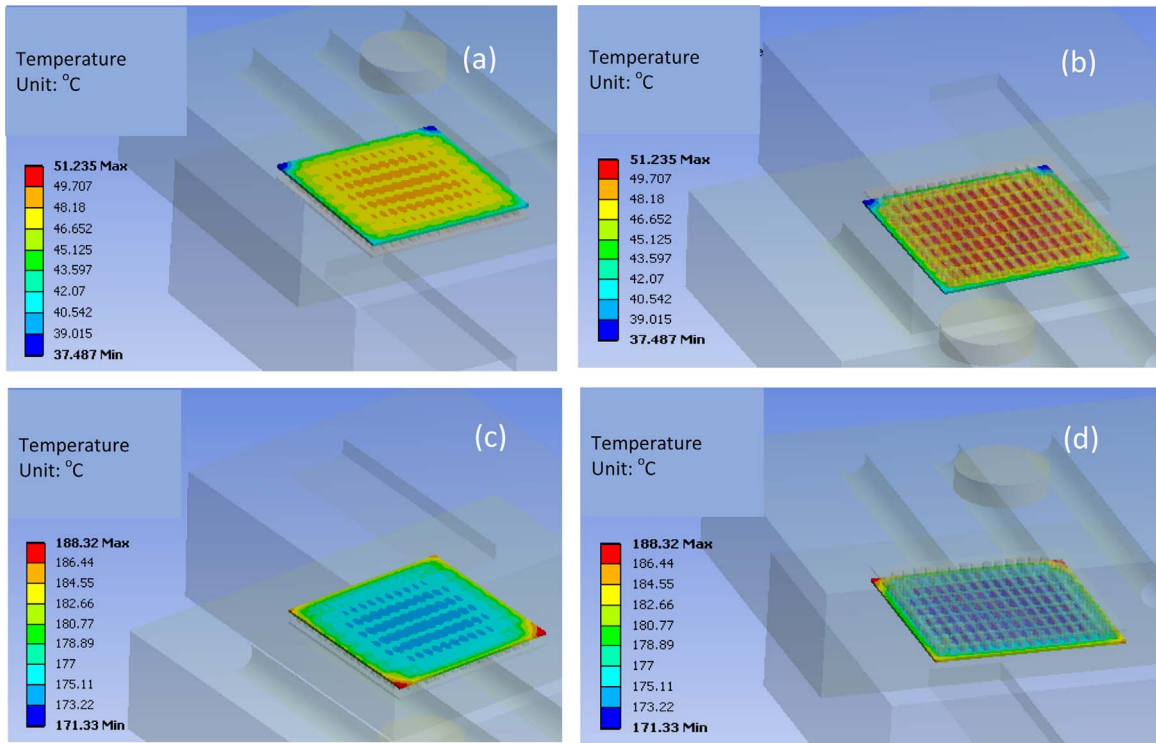


Fig. 8. Temperature contours on two surfaces of hot and cold substrates at  $\Delta T=150\text{ }^{\circ}\text{C}$  and  $I=2.4\text{ A}$ , (a) the surface contacted with the cold block, (b) the surface contacted with the straps in the cold side, (c) the surface contacted with the hot block, (d) the surface contacted with the straps in the hot side.

### 3.4. The other detailed variables in steady-state condition

The detailed performance parameters include the temperature contours on the hot and cold blocks, TEG module substrates, TEG elements and electrical variable profiles in the TEG circuit. These parametric distributions provide some physical insights into the performance of a TEG module. Since the temperature contours on the hot and cold blocks, the voltage, total current density and Joule heat profiles in the TEG circuit have been presented in [27], thus they no longer repeated here.

Instead, the temperature contours on the cold and hot substrate surfaces of the TEG module at  $\Delta T=150\text{ }^{\circ}\text{C}$  and  $I=2.4\text{ A}$  are shown in Fig. 8. It can be seen that two substrate surfaces in the cold and hot sides are subject to a non-uniform temperature profile, especially in the contacted areas between the straps (tabs) and the substrates. This is caused by the thermal contact effect, resulting in a temperature drop. Additionally, at the corners of the hot substrate, there are temperature concentrations, while at the corners of the cold substrate, there exists a sharp temperature declination.

### 3.5. Quasi-steady thermal response

Note that the thermal and electrical dynamics of a TEG have different time constants. The electrical response time is in the order of nano-seconds [37], thus the TEG converts thermal energy into electricity instantaneously [17]. The inductive and capacitive effects in a TEG are investigated in [38] and in most cases they can be neglected [20]. On the other hand, the thermal dynamic timescale is in the order of minutes [28,29]. To account for this prolonged timescale, the thermal response can be treated as a series of steady-state responses, i.e. a quasi-steady. To confirm this, transient and quasi-steady thermal analyses without any electrical couples were carried out in the TEG module under the same input condition as shown in Fig. 2(a). It is found that the temperature on both the hot and cold substrates in the transient case exhibits no difference compared with the quasi-steady case. Hence to consider the transient performance of a TEG module as an evolution of a series of steady-state solutions under various heater temperatures and electrical currents in the lead is reasonable.

## 4. Conclusions

This work studies the dynamic thermal and electrical performance of a TEG module placed between a hot block heated by an electrical heater, and a water-cooled block. ANSYS 15.0 is used to perform the numerical thermal-electrical analysis. The radiation, thermal and electrical contact effects have been investigated under both transient and steady-state operating conditions. The performance curves and parameters of the TEG are presented, and it is identified that the simulated transient and steady-state performance curves are in agreement with the experimental data. A new correlation for the Seebeck coefficient to temperature is also

proposed. The radiation effect is found to be negligible. The length of TEG's leg exhibits a significant effect on electrical performance, but its effect on the thermal performance can be neglected. The temperature predicted on the interfaces between the cold and hot blocks with the TEG's substrates is not perfectly uniform. The temperature profile along TEG leg is nearly linear.

## Acknowledgement

The work is supported by EPSRC SUPERGEN Solar Challenge with grant: EP/K022156/1-Scalable Solar Thermoelectrics and Photovoltaics (SUNTRAP). The support is appreciated very much.

## References

- [1] X. Py, Y. Azoumah, R. Olives, Concentrated solar power: current technologies, major innovative issues and applicability to West African countries, *Renew. Sustain. Energy Rev.* 18 (2013) 306–315.
- [2] H.P. Garg, R.S. Adhikari, Performance analysis of a hybrid photovoltaic/thermal (PV/T) collector with integrated CPC troughs, *Int. J. Energy Res.* 23 (1999) 1295–1304.
- [3] M.Y.H. Othman, B. Yatim, K. Sopian, M.N.A. Bakar, Performance analysis of a double-pass photovoltaic/thermal (PV/T) solar collector with CPC and fins, *Renew. Energy* 30 (2005) 2005–2017.
- [4] M.Y. Othman, B. Yatim, K. Sopian, M.N.A. Bakar, Performance studies on a finned double-pass photovoltaic-thermal (PV/T) solar collector, *Desalination* 209 (2007) 43–49.
- [5] T.T. Chow, W. He, J. Ji, Hybrid photovoltaic-thermosyphon water heating system for residential application, *Sol. Energy* 80 (2006) 298–306.
- [6] J. Ji, J.P. Lu, T.T. Chow, W. He, G. Pei, A sensitivity study of a hybrid photovoltaic/thermal water-heating system with natural circulation, *Appl. Energy* 84 (2007) 222–237.
- [7] Y. Deng, W. Zhu, Y. Wang, Y. Shi, Enhanced performance of solar-driven photovoltaic-thermo-thermoelectric hybrid system in an integrated design, *Sol. Energy* 88 (2006) 182–191.
- [8] R. Amatyia, R.J. Ram, Solar thermoelectric generator for micropower applications, *J. Electron. Mater.* 39 (2010) 1735–1740.
- [9] G.Q. Li, G. Pei, M. Yang, J. Ji, Y.H. Su, Optical evaluation of a novel static incorporated compound parabolic concentrator with PV/thermal system and preliminary experiment, *Energy Convers. Manag.* 85 (2014) 204–211.
- [10] T. Liao, B. Lin, Z. Yang, Performance characteristics of a low concentrated photovoltaic thermoelectric hybrid power generation device, *Int. J. Therm. Sci.* 77 (2014) 158–164.
- [11] C. Lertsatitthanakorn, Jamradloedluk, M. Rungsiyopas, Thermal modelling of a hybrid thermoelectric solar collector with a compound parabolic concentrator, *J. Electron. Mater.* 42 (7) (2013) 2119–2126.
- [12] A. Lineykin, S. Ben-Yaakov, Modeling and analysis of thermoelectric modules, *IEEE Trans. Ind. Appl.* 43 (2) (2007) 505–512.
- [13] M. Chen, L.A. Rosendahl, T.J. Condra, J.K. Pederson, Numerical modelling of thermoelectric generators with varying material properties in a circuit simulator, *IEEE Trans. Energy Convers.* 24 (1) (2009) 112–124.
- [14] F. Felgner, G. Frey, Object-oriented simulation model of thermoelectric devices for energy system design, in: *Proceedings of the 16th IEEE Mediterranean Electrotechnical Conference*, 25–28, March 2012, pp. 577–80.
- [15] H.L. Tsai, J.M. Lin, Model building and simulation of thermoelectric module using Matlab/Simulink, *J. Electron. Mater.* 39 (9) (2010) 2105–2111.
- [16] A.M. Yusop, R. Mohamed, A. Ayob, Model building of thermoelectric generator exposed to dynamic transient sources, in: *Proceedings of 5th International Conference on Mechatronics*, 2–4 July 2013, Kuala Lumpur, Malaysia, pp.1–9.
- [17] A. Montecucco, J.R. Buckle, A.R. Knox, Solution to the 1-D unsteady heat conduction equation with internal Joule heat generation for thermoelectric devices, *Appl. Therm. Eng.* 35 (2012) 177–184.
- [18] M. Alata, M.A. Al-Nimr, M. Naji, Transient behaviour of a thermoelectric device under the hyperbolic heat conduction model, *Int. J. Thermophys.* 24 (6) (2003) 1753–1768.
- [19] N.Q. Nguyen, K.V. Pochiraju, Behavior of thermoelectric generators exposed transient heat sources, *Appl. Therm. Eng.* 51 (2013) 1–9.
- [20] E.E. Antonova, D.C. Looman, Finite elements for thermoelectric device analysis in ANSYS, in: *Proceedings of the 24th International Conference on Thermoelectrics*, 19–23 June, 2005, pp. 215–2218.
- [21] K.H. Lee, O.J. Kim, Analysis on the cooling performance of the thermoelectric micro-cooler, *Int. J. Heat. Mass Transf.* 50 (2007) 1982–1992.
- [22] O. Hogblom, R. Andersson, Analysis of thermoelectric generator performance by use simulations and experiments, *J. Electron. Mater.* 43 (2014) 2247–2254.
- [23] W.H. Chen, C.Y. Liao, C.I. Hung, A numerical study on the performance of miniature thermoelectric cooler affected by Thomson effect, *Appl. Energy* 89 (2012) 464–473.
- [24] J.S. Xiaoi, T.Q. Yang, P. Li, P.C. Zhai, Q.J. Zhang, Thermal design and management for performance optimization of solar thermoelectric generator, *Appl. Energy* 93 (2012) 33–38.
- [25] S.L. Li, C.K. Liu, C.Y. Hsu, M.C. Hsieh, M.J. Dai, S.T. Wu, Thermo-mechanical analysis of thermoelectric modules, in: *Proceedings of the 5th International Microsystems Packaging Assembly and Circuits Technology Conference (IMPACT)*, Taipei, China, 20–22 October, 2010, pp. 1–4.
- [26] S. Turenne, Clin Th, D. Vasilevskiy, Masut R A, Finite element thermomechanical modelling of large area thermoelectric generators based on bismuth telluride alloys, *J. Electron. Mater.* 39 (2010) 1926–1933.
- [27] W. Li, M.C. Paul, A. Montecucco, et al., Multiphysics simulations of a thermoelectric generator, *Energy Procedia* 75 (2015) 633–638.
- [28] A. Montecucco, J. Buckle, J. Siviter, A.R. Knox, A new test rig for accurate nonparametric measurement and characterization of thermoelectric generators, *J. Electron. Mater.* 42 (2013) 1966–1973.
- [29] A. Montecucco, A.R. Knox, Accurate simulation of thermoelectric power generating systems, *Appl. Energy* 118 (2014) 166–172.
- [30] S.B. Riffat, X. Ma, R. Wilson, Performance simulation and experimental testing of a novel thermoelectric heat pump system, *Appl. Therm. Eng.* 26 (2006) 494–501.
- [31] W. Li, M.C. Paul, et al., Thermal performance of two heat exchangers for thermoelectric generators, *Case Stud. Therm. Eng.* 6 (2016) 164–175.
- [32] J.H. Lienhard IV, V.J.H. Lienhard, A Heat Transfer Textbook, 3rd edition, Phlogiston Press, Cambridge, Massachusetts, USA, 2008.
- [33] O. Yamashita, Effect of interface layer on the cooling performance of a single thermoelement, *Appl. Therm. Eng.* 88 (2011) 3022–3029.
- [34] F. Cheng, Y. Hong, C. Zhu, A physical model for thermoelectric generators with and without Thomson heat, *ASME J. Energy Recour. Technol.* 136 (2014) (pp.011201-011201).
- [35] L. Fan, G. Zhang, R. Wang, K. Jiao, A comprehensive and time-efficient model for determination of thermoelectric generator length and cross-section area, *Energy Convers. Manag.* 122 (2016) 85–94.
- [36] R. Bjork, D.V. Christensen, D. Eriksen, N. Pryds, Analysis of the internal heat losses in a thermoelectric generator, *Int. J. Therm. Sci.* 85 (2014) 12–20.
- [37] L. Chen, D. Cao, H. Yi, F.Z. Peng, Modeling and power conditioning for thermoelectric generation, in: *Power electronics specialists conference, IEEE*, 2008, pp. 1098–1103.
- [38] A. Montecucco, A.R. Knox, Maximum power point tracking converter based on the open-circuit voltage method for thermoelectric generators, *IEEE Trans. Power Electron* 30 (2015) 828–839.